Metascience in Aerospace, 3(1): 15–27.
DOI: 10.3934/mina.2026002
Received date: 02 January 2026
Revised date: 23 January 2026
Accepted date: 02 February 2026
Published date: 27 February 2026

https://www.aimspress.com/journal/mina

Research article

Quantification of uncertainty propagation for transient heat transfer in a hollow cylinder

Rama Subba Reddy Gorla* and Lochlan Joyce

Department of Aeronautics and Astronautics, Air Force Institute of Technology, Dayton, OH 45433, USA

* **Correspondence:** Email: rama.gorla@afit.edu.

Abstract: Uncertainty propagation in transient heat transfer for radial hollow cylinders was analyzed. The outer surface was assumed to be isothermal, and the inner surface was subjected to a convective boundary condition. The temperature distribution within the hollow cylinder was characterized by a stochastic Biot number, stochastic linear nondimensional initial conditions, and various boundary conditions. The resulting uncertainty amplitude exhibited transient temporal evolution. Depending on the stochastic parameters, uncertainty can either increase or decrease. Results are presented for the variation of temperature due to uncertainties in the initial conditions and selected boundary conditions.

Keywords: uncertainty; transient; heat conduction; hollow cylinder

Nomenclature

Bi_i = Biot number, $\frac{h_i r_i}{k}$
Bi_μ = mean value for stochastic quantity Bi
F_0 = dimensionless initial temperature at inner radius, $\theta(r^* = 0, \tau = 0)$
$F_{0\mu}, F_{1\mu}$ = mean values for stochastic quantities F_0, F_1
F_1 = dimensionless constant parameterizing initial temperature variation across l
h = heat transfer coefficient, $\frac{W}{m^2 K}$
$J_n = n^{th}$ order cylindrical Bessel function of first kind

k = isotropic thermal conductivity of the plate, $\frac{W}{mk}$
L = domain length, $r_o - r_i$
Q_o= heat flux at outer radius
r = radial dimension, m
r_i, r_0 = inner and outer radii of hollow cylinder, respectively
r^* = radial dimensionless coordinate, $\frac{r-r_i}{L}$
T = temperature, K
T_{ref} = reference temperature, K
T_{init} = initial temperature, K
T_1 = constant parameterizing initial temperature variation across L, K
T_∞ = temperature of ambient medium, K
t = time, s
$Y_0 = = n^{th}$ order cylindrical Bessel function of second kind
α = thermal diffusivity, $\frac{m^2}{s}$
$\Delta\theta$ = dimensionless temperature difference
θ = dimensionless temperature
λ_n = eigenvalues
τ = dimensionless time, $\frac{\alpha t}{L^2}$
Subscripts
i = inner radius
$init$ = initial
n= eigenvalue indices
o = outer radius
μ = mean value

1. Introduction

Thermal management in military and civil aircraft is critical for improving performance and efficiency. Bertin and Cummings [1] discussed the primary challenges associated with heat dissipation in high-speed aircraft, particularly the extreme temperatures resulting from aerodynamic heating during high-speed flight.

In computational and experimental results, it is important to quantify result accuracy. Kline et al. [2] and Moffat [3] discussed uncertainties in experimental data. Celik et al. [4] discussed uncertainties in computational results. In general, uncertainties in numerical calculations arise due to thermophysical properties, initial conditions, and boundary conditions, among others. Often, these parameters are treated as ideal inputs, resulting in deterministic solutions in which uncertainty, which plays an important role in the design of systems, is neglected. As a result, predicting uncertainty limits is important to obtain improved insight into practical problems and to establish a reliable basis for comparison with experimental data.

Mendes et al. [5] studied the uncertainty due to input parameters in steady-state fluid flow and heat transfer problems. Uncertainty quantification in numerical simulations allows one to set the confidence intervals for predicted system behavior. Panasyuk and Yerkes [6] conducted a one-dimensional transient heat transfer in a thin plate with a constant heat flux boundary condition and

compared their results with a high-fidelity experimental model. That research explored the implications for thermal management of components, including electronics. Panasyuk and Yerkes [7] explored a mathematical model for uncertainty analysis and examined the temporal evolution of the stochastic characteristics.

Muff et al. [8] studied a thin plate with a constant temperature boundary condition on one surface and a convective boundary condition on the other, representative of a plate that may be present on a high-speed vehicle. Material properties in this model were represented by the Biot number, defined as the ratio of internal conduction resistance to external convective resistance. Uncertainty in material properties, the convective heat transfer coefficient (h), or initial temperature conditions are expected to propagate through the model during unsteady transient simulations. Gorla et al. [9,10] studied multi-input statistical variation in a simplified linear deterministic model of a dynamic heat-rejection extended surface region within a thermal management system. Dimensionless material properties were represented using the Biot number and Fin number. The transient response of fins is important in numerous engineering devices, including heat exchangers, clutches, motors, and railroad roller bearings.

The present work investigates multi-input statistical variation in heat rejection within a hollow-cylinder thermal management system. The dimensionless material properties of the system are represented by the Biot number. Uncertainty in material properties, convective heat transfer coefficient, and initial thermal conditions are expected to propagate through the model during transient heat rejection. The objective is to characterize the nondimensional temperature and heat flux and to identify the factors that have the highest risk of exceeding known thermal management limitations. A practical application of this study is the simulation of an aircraft fuel tank.

2. Analysis

Considering an internal burning propellant configuration, the governing energy equation may be written as follows [11]:

$$\frac{\partial T}{\partial t} = \frac{\alpha}{r}\frac{\partial}{\partial r}\left(r\frac{\partial T}{\partial r}\right) \tag{1}$$

We define the dimensionless variables

$$\theta = \frac{T(r,t)-T_\infty}{T_{init}-T_\infty}\,, \qquad r^* = \frac{r-r_i}{r_o-r_i}, \qquad \tau = \frac{\alpha t}{L^2} \tag{2}$$

The nondimensionalized energy equation may be written as

$$\frac{\partial \theta}{\partial \tau} = \frac{1}{\left|\left(\frac{m}{1-m}\right)+r^*\right|}\frac{\partial}{\partial r^*}\left(\left|\left(\frac{m}{1-m}\right)+r^*\right|\frac{\partial \theta}{\partial r^*}\right) \text{ for } r^* \in [0,1] \tag{3}$$

where $m = \frac{r_i}{r_0}$.

The initial condition will be assumed as

$$\theta(r^*, 0) = F_0 + F_1 r^* \tag{4}$$

Here, both F_0 and F_1 can be randomly sampled using the Monte Carlo technique. We consider an adiabatic boundary condition at the inner radius and a convective boundary at the outer radius.

The inner convective boundary condition is described by the following equation:

$$-k\left(\frac{dT}{dr}\right)|_{\{r=r_i\}} = h_i(T(r_i,t) - T_\infty) \tag{5}$$

Using $Bi_i = \frac{h_i r_i}{k}$, we arrive at the nondimensional inner boundary condition:

$$\left(\frac{d\theta}{dr^*}\right)|_{\{r^*=0\}} = \left(\frac{1-m}{m}\right) Bi_i\ (\theta(0,\tau) - 1) \tag{6}$$

The outer constant temperature boundary is simply $T = T_0$. This can be written in its nondimensional form as

$$\theta(1,\tau) = 0 \tag{7}$$

Separation of variables using $\theta(r^*,\tau) = R(r^*)\mathrm{T}(\tau)$ leads to the following time equation:

$$\frac{d\mathrm{T}}{d\tau} = -\lambda^2\mathrm{T}(\tau) \tag{8}$$

The radial equation in dimensional form reads as follows:

$$\frac{1}{r}\frac{d}{dr}\left(r\frac{dR}{dr}\right) + \lambda^2 R = 0 \tag{9}$$

The time equation has a solution of the form $\mathrm{T}(\tau) = Ae^{-\lambda^2\tau}$, where A is a constant.

The radial differential equation can be solved using Bessel functions assuming the general form:

$$R(r) = C_1 J_0(\lambda r) + C_2 Y_0(\lambda r) \tag{10}$$

where C_1 and C_2 are constants. The single-mode nondimensional temperature can be written as:

$$\theta_n(r,\tau) = \left[C_{1,n}J_0(\lambda_n r) + C_{2,n}Y_0(\lambda_n r)\right]e^{-\lambda_n^2\tau} \tag{11}$$

Applying the boundary conditions described and solving the system of equations above allows us to solve for the transcendental eigenvalue roots:

$$0 = Y_0(\lambda)\left[-\lambda J_1(\lambda\, m) + \frac{Bi_i}{m}J_0(\lambda\, m)\right] - J_0(\lambda)\left[-\lambda Y_1(\lambda\, m) + \frac{Bi_i}{m}Y_o(\lambda\, m)\right] \tag{12}$$

To satisfy both the initial and boundary conditions, $\theta_n(r,\tau)$ is written as a summation of all eigenfunctions:

$$\theta_n(r,\tau) = \sum_{n=1}^{\infty} a_n R(r) e^{-\lambda_n^2\tau} \tag{13}$$

Finally, the last part of this equation that needs to be computed is a_n, which is determined by projecting the initial condition $\theta(r^*,0) = F_0 + F_1\, r^*$ onto the eigenfunctions by:

$$a_n = \frac{\int_0^1 \theta(r^*,0)R(r^*)\left[1+\left(\frac{1-m}{m}\right)r^*\right]dr^*}{\int_0^1 (R(r^*))^2\left[1+\left(\frac{1-m}{m}\right)r^*\right]dr^*} \tag{14}$$

Here, a_n was numerically solved using MATLAB.

The nondimensional temperature difference across the inner and outer faces of the hollow cylinder is given by

$$\Delta\theta = \theta(0,\tau) - \theta(1,\tau) \tag{15}$$

3. Stochastic simulation

After the development of the expression of the nondimensional temperature difference across the shell ($\Delta\theta$) and the nondimensional heat flux at the outer surface of the hollow cylinder ($\theta'(1,\tau)$), Monte Carlo simulations were conducted to observe the behavior of the system when uncertainty was introduced to various parameters. The main purpose of stochastic solutions is to determine the mean solution and to obtain the solution confidence interval for uncertainty in initial and boundary conditions.

The three variables that had uncertainty introduced to them are the Biot number (Bi), the dimensionless constant describing initial temperature at the inner surface (F_0), and the dimensionless constant parameterizing initial temperature variation across the hollow cylinder (F_1). For each term, a normal distribution was randomly generated with a standard deviation scaled appropriately to have 3 standard deviations represent ±10% variation in the term. In the Monte Carlo simulation, 100 random values were sampled for Bi, F_0, and F_1. All parameters are stochastic in every case. These conditions were implemented into Equations (12)–(15) to generate the results, which were then plotted against nondimensional time from 0 to 1000. A computer program was used to iterate calculations to find eigenvalues for each randomly selected Biot number.

4. Results

After several simulations, data were collected and plotted against nondimensional time. In all the figures shown, the time starts from $\tau = 0.01$ instead of 0 because of the logarithmic scale used. The key parameters that are varied are the Biot number, Bi_μ, and the constants $F_{0\mu}$ and $F_{1\mu}$. This provides a broad scope of material and temperature conditions that may be expected in both subsonic and high-speed flow heat exchange scenarios. The results section is divided into two parts for comparison of the temperature change across the surfaces as well as the heat flux at the outer surface.

4.1. Nondimensional temperature difference ($\Delta\theta$) *across the surfaces*

Figures 1–3 display the nondimensional temperature changes across the hollow cylinder surfaces as nondimensional time progresses. With increasing Biot number, the general behavior of the nondimensional temperature differences follows a similar trend. For all cases, the transient portion of this simulation lasts until a nondimensional time of $\tau = 1$. Beyond that point, there is a distribution of outputs, but its magnitude is much lower than the uncertainty observed during the earlier period in each simulation. In the later stages of the simulation, the output distribution is approximately uniform.

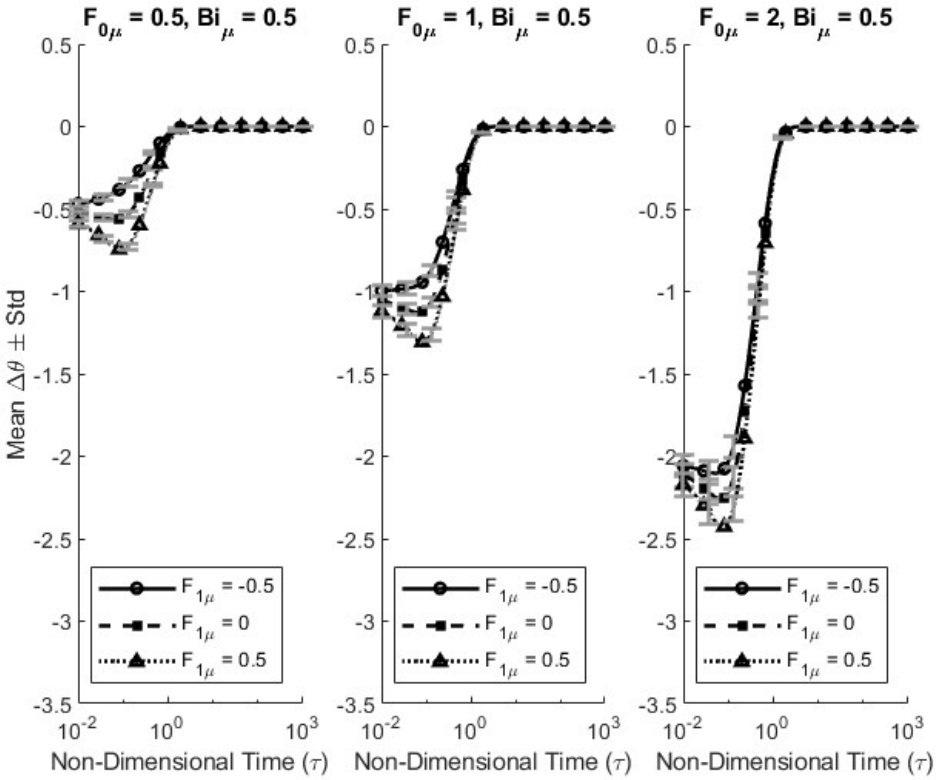

Figure 1. Evolution of $\Delta\theta$ versus τ with $Bi_\mu = 0.5$ and varying $F_{0\mu}$ and $F_{1\mu}$.

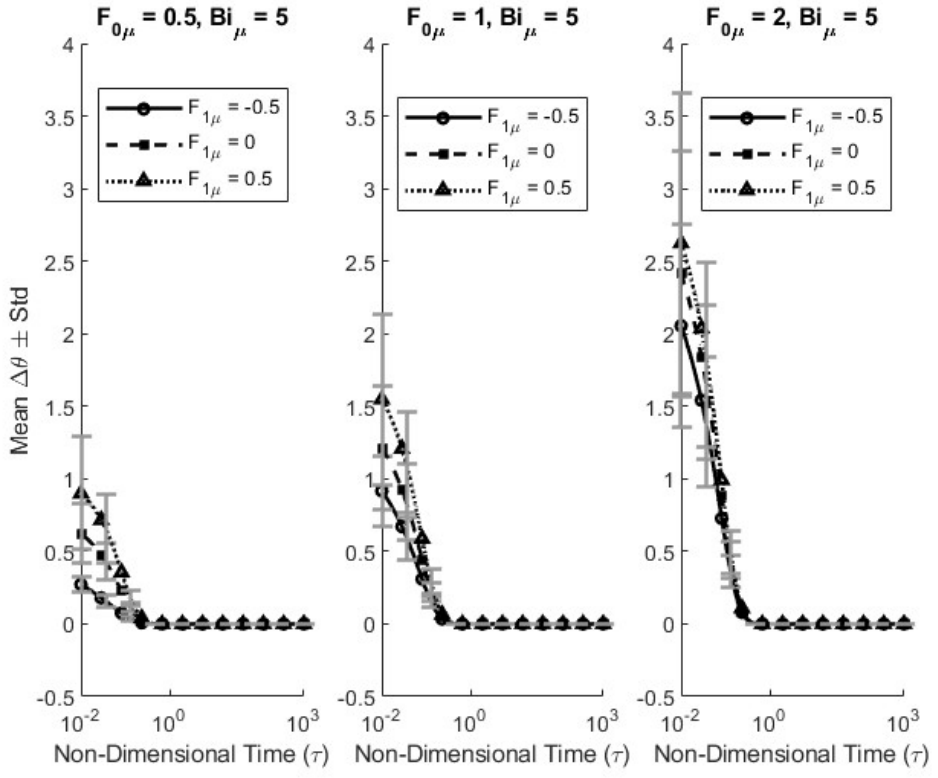

Figure 2. Evolution of $\Delta\theta$ versus τ with $Bi_\mu = 5$ and varying $F_{0\mu}$ and $F_{1\mu}$.

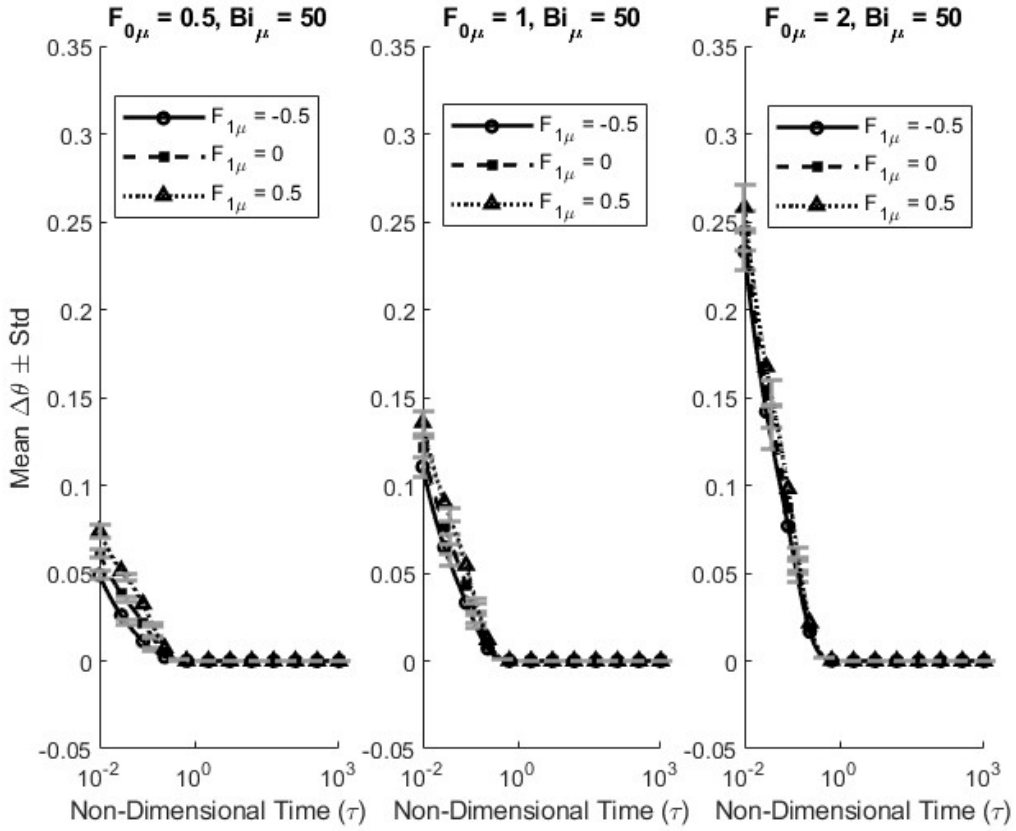

Figure 3. Evolution of $\Delta\theta$ versus τ with $Bi_\mu = 50$ and varying $F_{0\mu}$ and $F_{1\mu}$.

The simulations can be compared by varying $F_{0\mu}$ and $F_{1\mu}$ individually. Across the 45 simulations performed for $\Delta\theta$, changes in $F_{1\mu}$ produce minimal variation in the stochastic spread. Different values of $F_{1\mu}$ have a greater impact on the initial values of $\Delta\theta$, therefore affecting the transient path of the simulation. On the other hand, as $F_{0\mu}$ increases, the amount of uncertainty in the transient results also increases. This is most obvious for small Biot numbers, such as $Bi = 0.5$, as depicted in Figure 1. In this case, the range of variation in $\Delta\theta$ increases from approximately -0.5 to 0 when $F_{0\mu} = 0.5$ to approximately -2 to 0 when $F_{0\mu} = 2$. This becomes less apparent as the Biot number increases, since the magnitude of the Biot number drives the nondimensional temperature difference across the cylindrical surfaces.

4.2. Nondimensional heat flux $\boldsymbol{\theta'(1,\tau)}$ at the outer surface

The parameters used for the nondimensional heat flux are the same as those used for the nondimensional temperature differences across the plate. Figures 4–6 are organized similarly to the ones above.

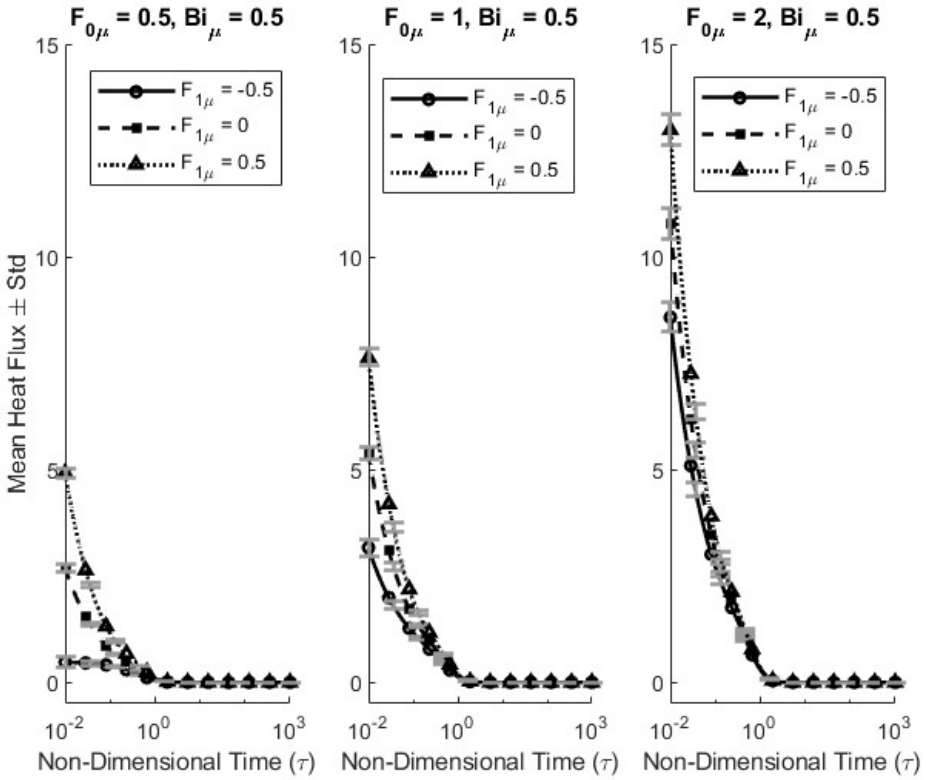

Figure 4. Evolution of $\theta'(1,\tau)$ versus τ with $Bi_\mu = 0.5$ and varying $F_{0\mu}$ and $F_{1\mu}$.

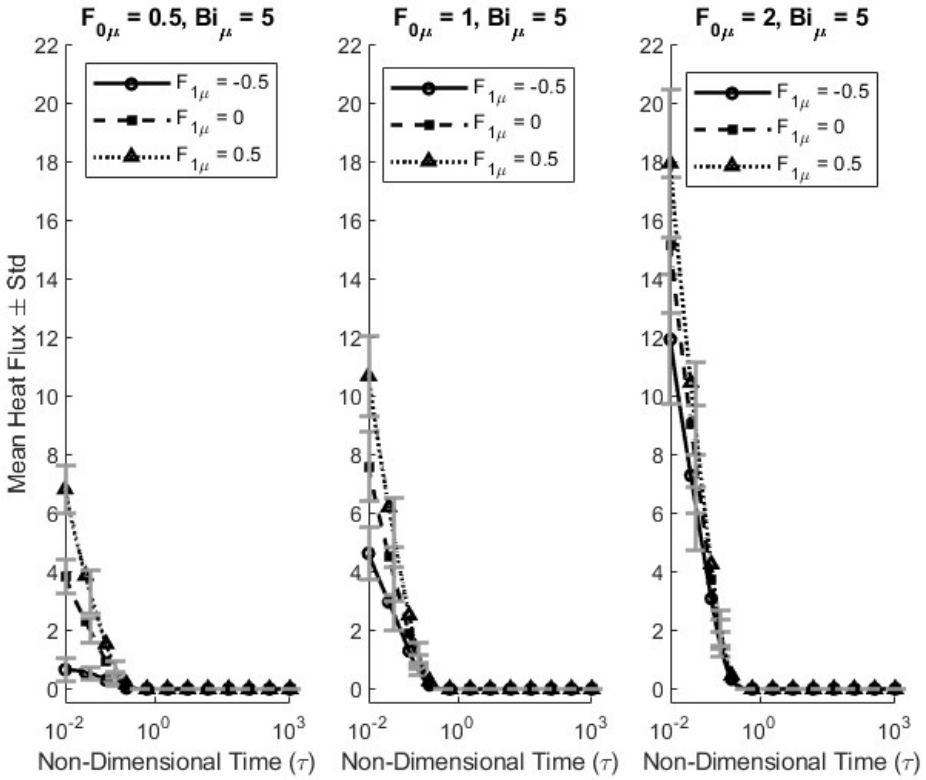

Figure 5. Evolution of $\theta'(1,\tau)$ versus τ with $Bi_\mu = 5$ and varying $F_{0\mu}$ and $F_{1\mu}$.

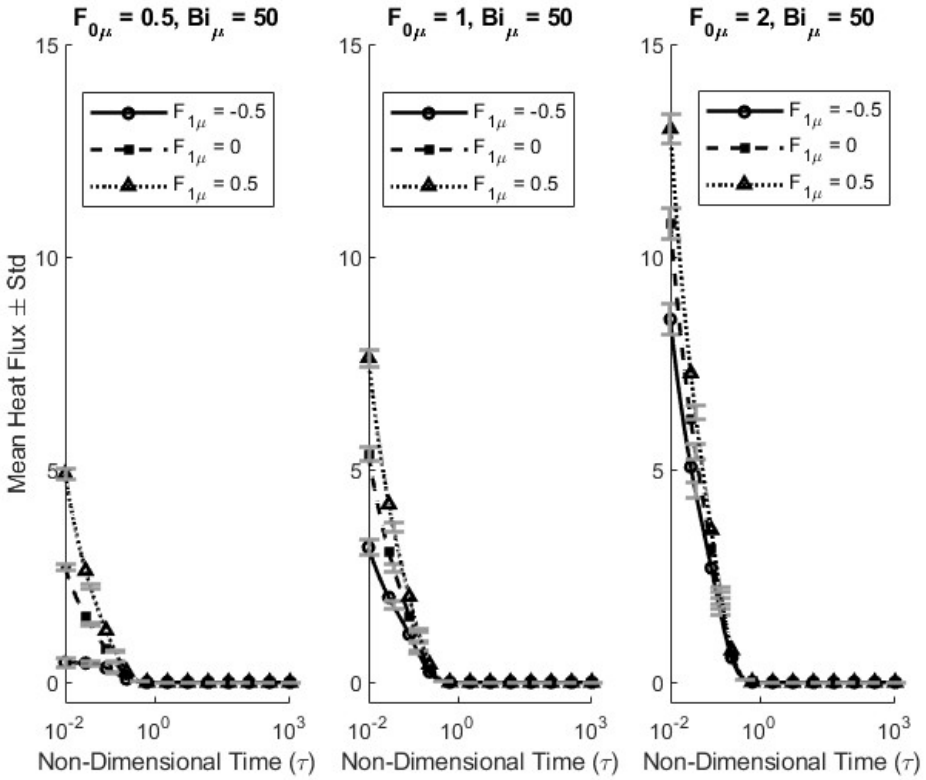

Figure 6. Evolution of $\theta'(1,\tau)$ versus τ with Bi_μ = 50 and varying $F_{0\mu}$ and $F_{1\mu}$.

In these simulations, the total uncertainty remains relatively consistent as the Biot number varies. The value of $F_{1\mu}$ has little effect on the overall uncertainty of the transient response; instead, it impacts the initial condition and path of the transients.

In contrast, the effect of $F_{0\mu}$ on $\theta'(1)$ is significantly more pronounced. For $F_{0\mu} = 0.5$, the uncertainty in $\theta'(1)$ is relatively low, and the general trend is an exponential decay with exclusively negative values. When $F_{0\mu} = 2$, the uncertainty in $\theta'(1)$ increases, still exhibiting exponential decay; however, in this case, all values of $\theta'(1)$ are positive. This suggests that the $F_{0\mu}$ term drives the direction of heat flux in these simulations.

For the third case (B_i = 50) with $F_{0\mu} = 0.5$, the simulations provide much more variation in the outputs. The uncertainty in the initial value of $\theta'(1)$ is sufficiently large that the direction of heat flux may vary, even when all other conditions are held constant. This variability quickly diminishes, and the final value reaches a constant by nondimensional time $\tau = 1$. This uncertainty in the direction of heat flux may have further implications when applied to a real-life system.

4.3. Nondimensional temperature $\boldsymbol{\theta(0,\tau)}$ at the inner surface

The parameters used for the nondimensional temperature are the same as those used for the nondimensional temperature differences across the plate. Figures 7–9 are organized similarly to the ones above.

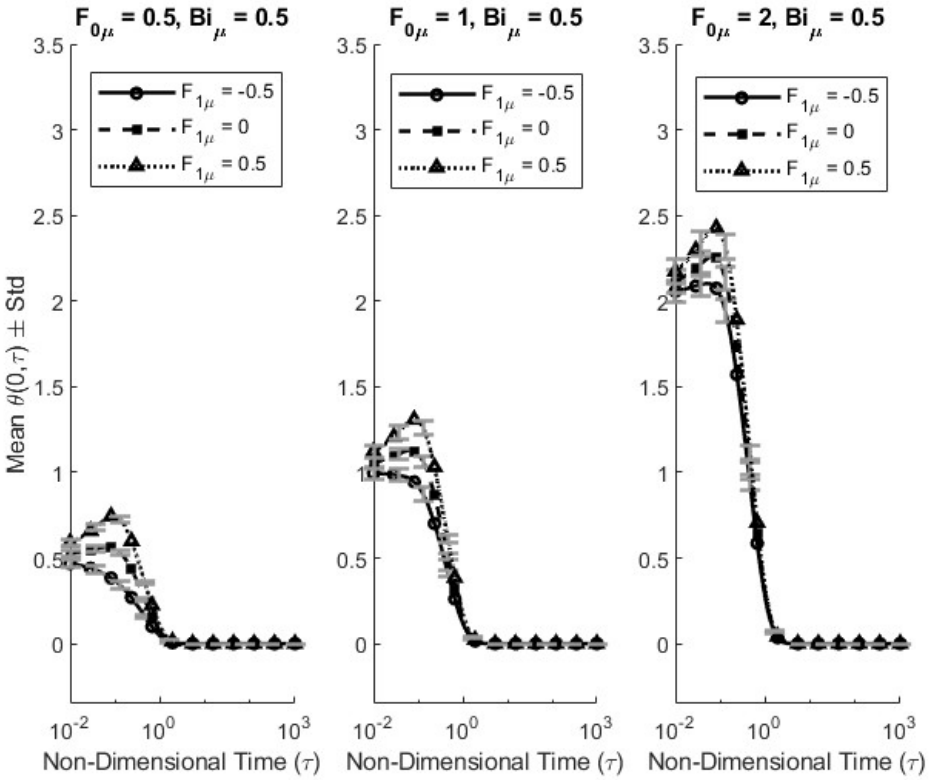

Figure 7. Evolution of $\theta(0,\tau)$ versus τ with $Bi_\mu = 0.5$ and varying $F_{0\mu}$ and $F_{1\mu}$.

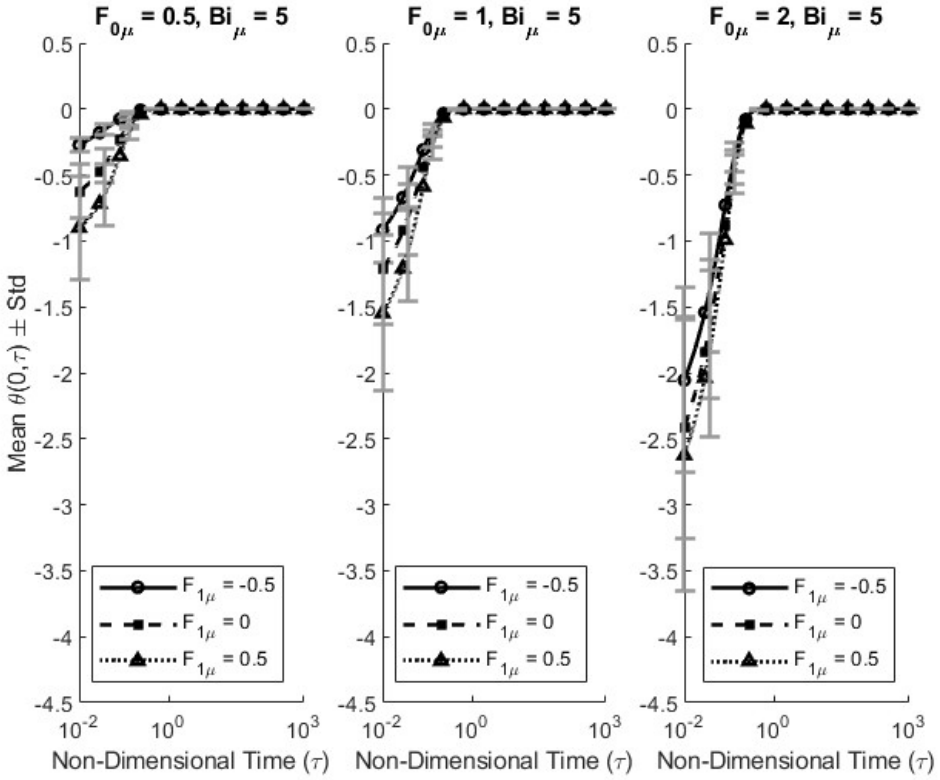

Figure 8. Evolution of $\theta(0,\tau)$ versus τ with $Bi_\mu = 5$ and varying $F_{0\mu}$ and $F_{1\mu}$.

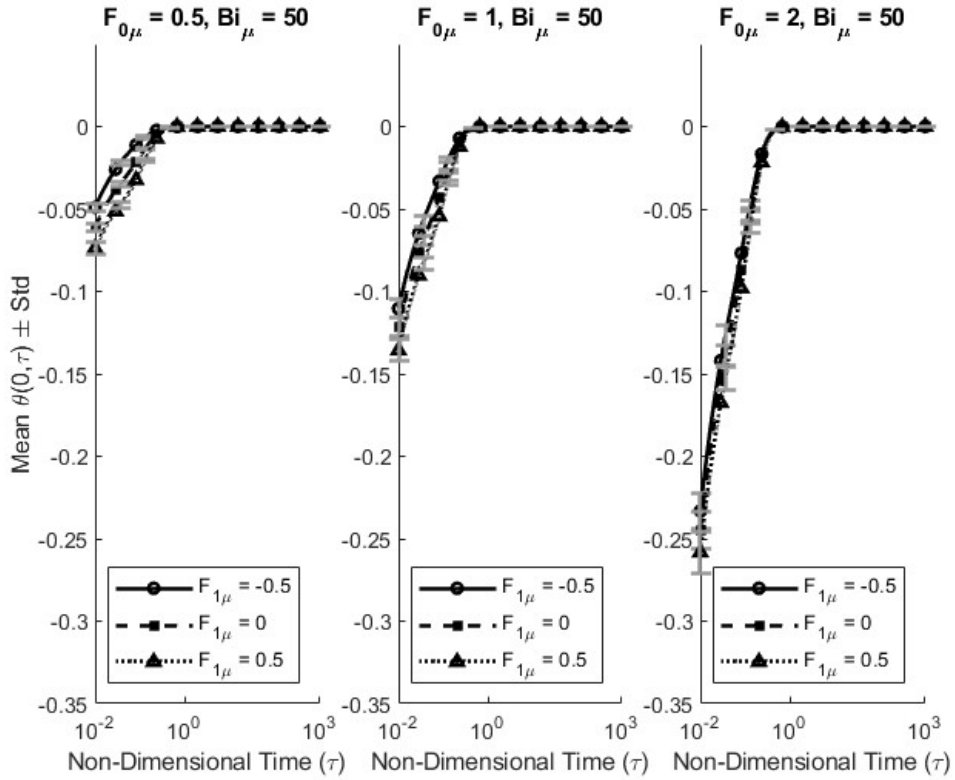

Figure 9. Evolution of $\theta(0,\tau)$ versus τ with Bi_μ = 50 and varying $F_{0\mu}$ and $F_{1\mu}$.

In these simulations, the total uncertainty remains relatively consistent as the Biot number changes. $F_{1\mu}$ has a minimal effect on the overall uncertainty of the transient response; instead, it impacts the initial condition and path of the transients.

There is a much more significant effect of $F_{0\mu}$ on $\theta(0)$. With values of $F_{0\mu} = 0.5$, the uncertainty in $\theta(0)$ is relatively low, and the general trend is an exponential decay with exclusively negative values. When $F_{0\mu} = 2$, the uncertainty in $\theta(0)$ is high, following an exponentially decaying trend.

5. Concluding remarks

Following multiple Monte Carlo simulations of the one-dimensional hollow-cylinder system, the transient thermal management behavior was documented and displayed. Uncertainty in the Biot number and in the initial conditions influenced the overall behavior of the interaction; however, all simulations followed an exponentially decaying trend that ultimately reached a steady-state value with a small, uniform distribution. Throughout each simulation, uncertainty continuously decreased as time progressed.

The greatest variability in $\Delta\theta$ occurred for higher values of $F_{0\mu}$, particularly at low Biot numbers. The largest variability in $\theta'(1)$ was observed when $F_{1\mu} = 0.5$. In many cases, uncertainty in the Biot number and initial conditions produced both positive and negative outputs, resulting in an unknown direction of heat flux in the system. This is a critical consideration in the design of high-speed aircraft and associated cooling systems.

Uncertainty propagation (UP) must be incorporated into the design to more accurately represent the effects of flow on structures. UP-based design formally quantifies the effect of uncertainties. It is essential to strengthen structural UP capabilities to account for aerodynamic and heat transfer uncertainties. The objective is to develop non-deterministic UP design tools that improve speed, accuracy, intelligence, and usability of the system in early-stage design.

This research can be extended to examine unsteady two-dimensional heat transfer problems for more practical applications of real-life heat exchangers.

Author contributions

Dr. Gorla formulated the problem, analyzed the results and wrote the manuscript. Mr. Joyce helped with numerical data collection.

Use of AI tools declaration

The authors declare they have not used Artificial Intelligence (AI) tools in the creation of this article.

Acknowledgements

The authors are supported by funding from the Fund for Scientific Research, Flanders (FWO, Belgium, G.0221.12), the Fondation Leducq (MIBAVA – Leducq 12CVD03). BL is senior clinical investigator of the Fund for Scientific Research, Flanders and holds a starting grant from the European Research Council (ERC-StG-2012-30972-BRAVE).

Conflict of interest

The authors declare no conflict of interest.

References

1. Bertin JJ, Cummings RM (2021) *Aerodynamics for Engineers*, Cambridge University Press. https://doi.org/10.1017/9781009105842
2. Kline SJ (1963) Describing Uncertainties in Single-Sample Experiments. *Mech Eng* 75: 3–8.
3. Moffat RJ (1988) Describing the Uncertainties in Experimental Results. *Exp Therm Fluid Sci* 1: 3–17. https://doi.org/10.1016/0894-1777(88)90043-X
4. Celik I, Chen CJ, Roache PJ, et al. (1993) *Quantification of Uncertainty in Computational Fluid Dynamics*, ASME Fluids Engineering Division Summer Meeting, Washington DC, 20–24.
5. Mendes MAA, Ray S, Pereira JMC, et al. (2012) Quantification of Uncertainty Propagation due to Input Parameters for Simple Heat Transfer Problems. *Int J Thermal Sci* 60: 94–105. https://doi.org/10.1016/j.ijthermalsci.2012.04.020

6. Panasyuk GY, Yerkes KL (2022) Input Uncertainty and Implication for Modeling Generic and High-Fidelity Transient Convection Problems. *J Thermophys Heat Transfer* 36: 1025–1034. https://doi.org/10.2514/1.T6444
7. Panasyuk GY, Yerkes KL (2024) Modeling of Uncertainty Propagation for Transient Heat Rejection Problems. *J Thermophys Heat Transfer* 38: 181–189. https://doi.org/10.2514/1.T6820
8. Muff JD, Gorla RSR, Forster E (2025) Uncertainty Quantification for Transient Thermal Management. *J Adv Therm Fluid Syst Aerosp* 1: 9–17. https://doi.org/10.2514/6.2025-3341
9. Gorla RSR, Forster E, Pentecost B (2025) Uncertainty Propagation in Transient Heat Transfer from an Extended Surface. *Int J Turbo Jet Eng* 42: 779–792. https://doi.org/10.1515/tjj-2025-0019
10. Gorla RSR, Pentecost B, Forster E (2025) Quantification of Uncertainty Propagation in Transient Heat Transfer from Flux-base Extended Surface. *Int J Turbo Jet Eng* 42: 807–824. https://doi.org/10.1515/tjj-2025-0029
11. Carslaw HS, Jaeger JC (1986) *Conduction of Heat in Solids*, Oxford University Press.

AIMS Press